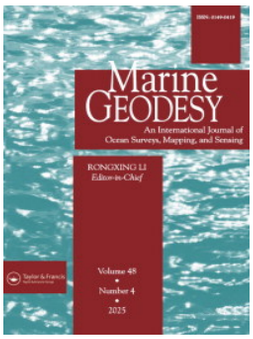

Marine Geodesy

ISSN: 0149-0419 (Print) 1521-060X (Online) Journal homepage: www.tandfonline.com/journals/umgd20

Development of an Ellipsoid Based Chart Datum Around the China Seas

Yanguang Fu, Yanxiong Liu, Mehdi Khaki, Fukai Peng, Xiaolong Mi, Yikai Feng, Xiaoli Deng, Long Yang, Qinghua Tang & Li Cui

To cite this article: Yanguang Fu, Yanxiong Liu, Mehdi Khaki, Fukai Peng, Xiaolong Mi, Yikai Feng, Xiaoli Deng, Long Yang, Qinghua Tang & Li Cui (2025) Development of an Ellipsoid Based Chart Datum Around the China Seas, Marine Geodesy, 48:4, 452-475, DOI: 10.1080/01490419.2025.2479618

To link to this article: https://doi.org/10.1080/01490419.2025.2479618

Published online: 08 Apr 2025.

MARINE GEODESY
2025, VOL. 48, NO. 4, 452–475
https://doi.org/10.1080/01490419.2025.2479618

Taylor & Francis
Taylor & Francis Group

Development of an Ellipsoid Based Chart Datum Around the China Seas

Yanguang Fu[a], Yanxiong Liu[a], Mehdi Khaki[b], Fukai Peng[c], Xiaolong Mi[d], Yikai Feng[a], Xiaoli Deng[b], Long Yang[a], Qinghua Tang[a], and Li Cui[a]

[a]First Institute of Oceanography, Ministry of Natural Resources, Qingdao, China; [b]School of Engineering, The University of Newcastle, Callaghan, New South Wales, Australia; [c]School of Geospatial Engineering and Science, Sun Yat-Sen University, Guangzhou, China; [d]Department of Land Surveying and Geo-Informatics, The Hong Kong Polytechnic University, Hong Kong

ABSTRACT

Establishing a continuous chart datum (CD) surface is essential for marine navigation and geodetic applications. In China, the theoretical lowest tide (TLT) surface is adopted as the CD, calculated using 13 specific tidal constituents. This study outlines a comprehensive methodology for constructing a continuous TLT surface referenced to the Chinese Geodetic Coordinate System 2000 (CGCS2000) ellipsoid around the China Seas. A high-precision hybrid tide model was developed by integrating global tide models with satellite altimetry data to ensure a reliable CD. Accuracy evaluations of four global tide models, based on 72 tide gauge observations, identified EOT20 as the optimal model. The hybrid tide model incorporates eleven short-period constituents from EOT20 and FES2014, and two long-period constituents empirically derived from along-track satellite data. Using this hybrid tide model, we first constructed a mean sea surface (MSS) based TLT model. By integrating the HYBRID2023MSS model, this study further established a CGCS2000-based TLT model. Validation against measurements from the 72 tide gauge stations revealed that the ellipsoid based TLT model produces ellipsoid heights ranging from −53.44 to 74.50 m, exhibiting significant spatial variation. The MSS based TLT model achieved a standard deviation of 14.68 cm, confirming its high accuracy and reliability for practical applications.

ARTICLE HISTORY
Received 3 November 2024
Accepted 10 March 2025

KEYWORDS
Chart datum; theoretical lowest tide; long-period tidal constituent; ocean tide model; satellite altimetry

Introduction

The determination of the continuous chart datum (CD) surface is crucial for establishing a vertical control datum for bathymetric reduction, spatial information representation and various maritime applications. It is predominantly utilized for sea level change analysis and vertical datum unification research

CONTACT Yanxiong Liu yxliu@fio.org.cn First Institute of Oceanography, Ministry of Natural Resources, Qingdao, China

(Turner et al. 2010). Recent studies indicate that while global ocean tide models exhibit high accuracy for the short-period tidal constituents, they often lack accuracy in providing long-period constituents' results (Cheng and Andersen 2011; Fok 2012). To address this limitation, satellite-derived long-period constituents have been proven to offer valuable insights, as they align more closely with tide gauge observations (Feng et al. 2023). Consequently, the creation of a hybrid model by integrating tide models and satellite-derived results presents an effective approach to achieving a precise CD surface.

Tide gauges have traditionally served as the primary tools for determining CD values. These tide gauge stations provide highly accurate measurements at shorter intervals, leading to more precise CD values. However, challenges arise in determining CD values through tide gauge observations. Firstly, while the CD surface signifies continuous seamless changes, the tide gauge-based values are spatially discrete, resulting in varying CD values for water depth reduction (Varbla et al. 2022). Secondly, the accuracy of CD determination is heavily reliant on the duration of tide gauge observations (Iz and Shum 2022). Longer observation periods yield more precise CD values, which may not be feasible for all tide gauge stations. Additionally, factors such as vertical land movement influence tide gauge instruments located in coastal, island, and deep-ocean stations. These factors cause the tide gauge observations to reflect relative sea level changes, leading to time-varying CD values (Avşar and Kutoğlu 2020).

Satellite altimetry techniques have advanced significantly, addressing many limitations of tide gauge observations. Satellites such as TOPEX/Poseidon (T/P) and the Jason series, operating in low Earth orbit with repeat tracks, provide precise and near-global measurements of sea level variability. These advancements have greatly improved our understanding of global tides. Extracting tidal constituent information from satellite altimetry data, as demonstrated by Pan et al. (2024) in the Bohai Sea using a modified tidal harmonic analysis algorithm, has garnered considerable interest. The along-track points of satellite altimetry serve as virtual tide gauge stations, providing continuous tide level data synchronized with satellite sampling time, particularly beneficial for regions with rarely tide gauge coverage. Azkue, Onofrio, and Banegas (2021) developed an empirical CD model for the Southwest Atlantic Ocean utilizing satellite-derived tidal harmonic constants from multiple missions. Continuous improvement in geophysical correction models, such as the wet tropospheric (Desportes, Obligis, and Eymard 2007; Madsen, Høyer, and Tscherning 2007), the waveform retracking technique (Deng and Featherstone 2006), and the X-TRACK method (Birol et al. 2017), has made satellite altimetry an indispensable tool for constructing accurate CD surface.

The aim of this research is to enhance the precision of the CD around the China Seas by integrating tide models with satellite-derived tidal constituents. The accuracy of modern CD models relies heavily on the tide models. Recent advancements in data processing have led to improvements in the accuracy of tide models (Stammer et al. 2014; Sun et al. 2022). However, current global tide models primarily focus on enhancing the accuracy of short-period tidal constituents, with less emphasis on long-period tidal constituents (Ray 1999; Cheng and Andersen 2011; Fok 2012). This emphasis on short-period constituents is due to their significant contribution to tidal levels, while long-period tidal constituents, influenced by factors like wind and pressure, are often disregarded due to their lower amplitudes and non-numerical nature.

The International Hydrographic Organization recommends using the lowest astronomical tide (LAT) as the CD surface, contrasting with the historical adoption of theoretical lowest tide (TLT) in China Seas. The TLT level corresponds to the lowest achievable theoretical tide level calculated based on 13 specific tidal constituents, that is, Q_1, O_1, P_1, K_1, N_2, M_2, S_2, K_2, M_4, MS_4, M_6, Sa, and Ssa. It is noteworthy that the majority of LAT datum models are developed without considering the effects of long-period tidal constituents (Turner et al. 2013). Research indicates that long-period tidal constituents can contribute up to 23.97% in the construction of TLT model in the China Seas (Feng et al. 2023), underscoring the critical importance of accounting for these constituents in the development of CD models.

The article is organized as follows: Section 2 outlines the data and methodology for determining TLT model. Section 3 elaborates on the construction of an empirical tide model integrating long-period tidal constituents derived from satellite data. Section 4 compares the accuracy of tide models. Section 5 establishes the TLT model. Section 6 discusses the precision and constraints of the TLT model, while Section 7 encapsulates the conclusions derived from this research endeavor.

Materials and methods

Tide gauge-derived tidal constituents

The study utilizes tidal harmonic constants to validate the CD model. A total of 72 long-term tide gauge stations are included in the harmonic constant dataset, strategically positioned across the study area defined by the geographical coordinates of 0° N–41° N latitude and 96° E–129° E longitude (Figure 1).

This dataset encompassed harmonic constants of 13 major tidal constituents, which include diurnal and semi-diurnal (Q_1, O_1, P_1, K_1, N_2, M_2, S_2, and K_2), shallow water constituents (M_4, MS_4, and M_6), as well as long-period

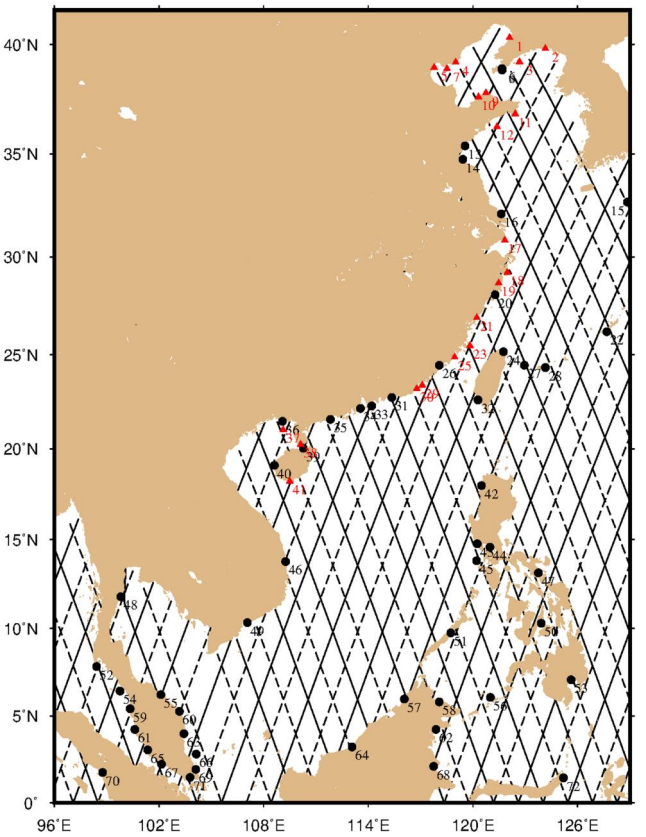

Figure 1. Distribution of tide gauge stations and satellite tracks in the study area. The Chinese tide gauge stations are denoted by red triangles, while the GESLA-3 stations are marked by black circles. The primary mission along-tracks of TOPEX/Poseidon and Jason are represented by solid lines, and the interleaved mission along-tracks are depicted by dotted lines.

constituents (Sa and Ssa). Notably, the tidal constants for 51 tide gauge stations are derived from TIdal CONstants (TICON; Piccioni et al. 2019), while data for the remaining 21 tide gauge records are sourced from the Chinese tide gauge station (CTG).

The TICON-3 dataset encompasses harmonic constants of 40 tidal constituents computed for 5119 tide gauges located on a quasi-global scale, along with additional details (Woodworth et al. 2016; Haigh et al. 2023). These tidal calculations are based on publicly accessible sea level data from the Global Extreme Sea Level Analysis (GESLA) project (https://gloss-sea-level.org/), presenting the most current and comprehensive high-frequency tide gauge data compiled from 33 international sources. The tidal constants were obtained from the GESLA-3 time series using a least-squares harmonic analysis method. A thorough screening process was conducted on all records to eliminate unreliable observations, ensuring that the time series utilized are longer than one year.

The CTG dataset contains three years of hourly sampled tide observations spanning from January 1, 2010 to December 31, 2012. The missing data and extreme values were interpolated using a continuous iteration method based on the least squares technique. This process yielded 13 tidal constituents mentioned above at 21 tide gauge stations. The amplitude and phase values of Sa and Ssa tidal constituents at each CTG station are detailed in Table 1.

It is worth noting that the observation period of the CTG dataset (2010–2012) does not coincide with that of the TICON-3 dataset or the satellite altimetry. Admittedly, this temporal discrepancy has some impact on the accuracy of the harmonic constants obtained, which in turn affects the evaluation results of this study. Previous researches have shown that when the time scale reaches 10 years or more, the standard error of Sa and Ssa tidal constituents can be reduced to below 1 cm (Feng et al. 2023). Nevertheless, on the one hand, it is virtually impossible for most tide gauge stations to obtain continuous tidal measurements over a period exceeding a decade. On the other hand, the uniform distribution of tide gauge stations is more beneficial for assessing the accuracy of the TLT model across different regions. Therefore, this study ultimately retains these tidal data to ensure comprehensive evaluation.

Tide models and satellite-derived tidal constituents

We use the grided harmonic constants from the FES2014, FES2022, EOT20, and DTU16 global ocean tide models, along with the satellite-derived tidal

Table 1. Geographic information and harmonic constants of annual (Sa) and semi-annual (Ssa) long-period tidal constituents in the Chinese tide gauge stations.

			Sa		Ssa	
Station No.	Lon (°)	Lat (°)	amp (cm)	pha (°)	amp (cm)	pha (°)
1	122.10	40.30	29.12	201.39	2.89	32.40
2	118.51	38.92	27.52	203.63	3.18	344.52
3	118.95	24.88	15.07	296.64	4.87	60.15
4	124.15	39.82	27.55	207.66	3.21	28.94
5	110.13	20.23	10.54	292.42	6.29	76.82
6	121.47	28.69	14.19	253.30	3.76	23.76
7	119.01	39.21	28.27	204.85	2.79	352.59
8	120.32	37.65	25.12	209.95	1.47	331.86
9	121.83	30.83	19.77	227.49	2.52	6.50
10	117.10	23.40	13.06	301.71	5.27	57.36
11	120.74	37.83	24.82	210.42	1.39	346.74
12	119.83	25.47	13.22	283.79	4.61	55.42
13	121.38	36.27	22.38	216.26	1.48	351.93
14	120.22	26.92	13.61	274.62	4.38	57.26
15	109.50	18.23	14.45	315.19	7.50	69.13
16	116.78	23.22	13.00	302.15	5.67	59.45
17	122.42	36.87	22.15	215.09	1.72	2.79
18	121.97	29.22	16.55	244.01	2.69	38.39
19	117.78	38.98	29.75	203.27	3.51	342.81
20	109.12	21.02	10.01	273.42	6.03	86.63
21	122.67	39.23	26.06	208.31	2.22	8.46

constituents obtained from the Centre of Topography of the Oceans and the Hydrosphere (CTOH). These selections were made based on their proven precision in monitoring global ocean areas and their superior spatial resolution. These models present the cutting edge in global tidal predictions. Refer to Table 2 for a detailed comparison of the resolution and tidal constituents included in the four global tide models, as well as the CTOH constituents.

FES2014 and FES2022, developed by Laboratory of Space Geophysics and Oceanography Studies (LEGOS) and NOVELTIS, utilize finite element methods to solve tidal dynamics equations, calibrated with satellite altimetry and tide gauge data (Lyard et al. 2006). These models encompass primary and secondary tidal constituents, capturing tidal variations globally. FES2014 offers superior spatial resolution and precision compared to earlier versions like FES2004 and FES2012, especially in regions with complex topography (Lyard et al. 2021). FES2022, an upgraded version of FES2014, further refines the computational and data processing techniques. The spatial resolution was increased from $1/16^\circ \times 1/16^\circ$ to $1/30^\circ \times 1/30^\circ$, as shown in Table 2.

Empirical Ocean Tide model 2020 (EOT20), developed by the GFZ German Research Centre for Geosciences, is a global tide model that integrates satellite altimetry data with extensive observational data to improve the accuracy of tidal predictions (Savcenko et al. 2012). It encompasses 17

Table 2. The resolution and tidal constituents of the four global ocean tide models, and CTOH constituents. The 13 common constituents among models are in bold.

Global ocean tide model					
		Tidal constituents			
Model	Resolution	Short-period			Long-period
FES2014	$1/16^\circ \times 1/16^\circ$	**K_1, O_1, P_1, Q_1**, S_1, J_1	**M_2**, E_2, **S_2**, **N_2**, **K_2**, R_2, T_2, L_2, $2N_2$, MKS_2, Nu_2, La_2, Mu_2	M_3, **M_4**, MN_4, N_4, **MS_4**, S_4, **M_6**, M_8	**Sa**, **Ssa**, Mf, Mm, Mtm, Msf, Msqm
FES2022	$1/30^\circ \times 1/30^\circ$	**K_1, O_1, P_1, Q_1**, S_1, J_1	$2N_2$, E_2, **M_2**, **S_2**, **N_2**, **K_2**, $2N_2$, MKS_2, T_2, La_2, R_2, Nu_2, L_2, Mu_2	M_3, **M_4**, MN_4, N_4, **MS_4**, S_4, **M_6**, M_8	**Sa**, **Ssa**, Mf, Mm, Mtm, Msf, Msqm
EOT20	$1/8^\circ \times 1/8^\circ$	**K_1, O_1, P_1, Q_1**, S_1, J_1	**M_2, S_2, N_2, K_2**, $2N_2$, T_2	**M_4**	**Sa**, **Ssa**, Mf, Mm
DTU16	$1/8^\circ \times 1/8^\circ$	**K_1, O_1, P_1, Q_1**	**M_2, S_2, N_2, K_2**	–	–
CTOH					
		Short-period			Long-period
Q_1, O_1, P_1, K_1, S_1, $2Q_1$, Sig_1, Ro_1, MP_1, M_1, J_1, Ki_1, Pi_1, Psi_1, Phi_1, Tta_1, SO_1, OO_1, KQ_1	**N_2, M_2, S_2, K_2**, OQ_2, MNS_2, La_2, R_2, $2MK_2$, $2N_2$, Mu_2, T_2, L_2, Nu_2, MSK_2, $2SM_2$, E_2, KJ_2, $M(SK)_2$, MSN_2, MKS_2, $M(KS)_2$		$2MK_3$, M_3, SO_3, MK_3, S_3, SK_3, MO_3, N_4, $3MS_4$, MN_4, **M_4**, SN_4, **MS_4**, MK_4, S_4, SK_4, $2MN_6$, **M_6**, MSN_6, $2MS_6$, $2MK_6$, $2SM_6$, MSK_6, $3MS_8$	**Sa**, **Ssa**, Msm, Mm, Msf, Mf, Mstm, Mtm, Msqm, Mqm

tidal constituents, providing detailed forecasts. Compared to its predecessors EOT11a and EOT10a, EOT20 exhibits notable enhancements in data processing and tidal constituent extraction, particularly in shallow water areas (Hart-Davis et al. 2021).

The DTU16 tide model, developed by the Technical University of Denmark (DTU), represents one of the latest advancements in global tide modeling (Cheng and Andersen 2011). It aims to provide high-precision tidal predictions and analysis. This model integrates extensive satellite altimetry data and tidal observations, using advanced numerical simulation methods and data assimilation techniques to accurately depict tidal variations across the global oceans. The DTU16 model includes harmonic constants for eight major tidal constituents with a relatively low spatial resolution of $1/8^\circ \times 1/8^\circ$.

The CTOH is a French Observation Service founded in 1989, specializing in satellite altimetry studies. Its primary goal is to enhance the accuracy of altimetric measurements and related products. CTOH provides a collection of 75 harmonic constants known as X-TRACK Coastal products. X-TRACK is designed as a regional altimeter product specifically tailored for coastal applications. The enhancements in the X-TRACK product and the increased precision in nearshore data are thoroughly examined and outlined by Birol et al. (2017). The along-track tidal constants, including amplitude, phase lags and associated estimation errors for 75 constituents, are derived from CTOH's along-track 1 Hz SLA products and computed through harmonic analysis of time series data from T/P, Jason-1 and Jason-2 satellite.

This study area encompasses 36 along-track passes from primary missions and 37 passes from interleaved missions. Figure 2 illustrates the along-track distribution of satellite-derived amplitude and phase of Sa and Ssa tidal constituents. In Section 3, the spatial distribution of the harmonic constants of the Sa and Ssa is analyzed in detail in the construction of the empirical model.

Calculation of theoretical lowest tide level

The TLT is calculated in accordance with the Chinese National Standard Specifications for Hydrographic Surveying (GB12327-2022) (National Standards of China 2023), which incorporates 13 tidal constituents.

$$\begin{aligned} L = -\min[&(fH)_{K_1}\cos\varphi_{K_1} + (fH)_{K_2}\cos(2\varphi_{K_1} + a_4) - R_1 - R_2 - R_3 + (fH)_{M_4}\cos\varphi_{M_4} \\ &+ (fH)_{MS_4}\cos\varphi_{MS_4} + (fH)_{M_6}\cos\varphi_{M_6} - H_{S_a}\left|\cos\varphi_{S_a}\right| + H_{S_{Sa}}\cos\varphi_{S_{Sa}}] \\ \varphi_K &\in [0^\circ \sim 360^\circ] \end{aligned} \tag{1}$$

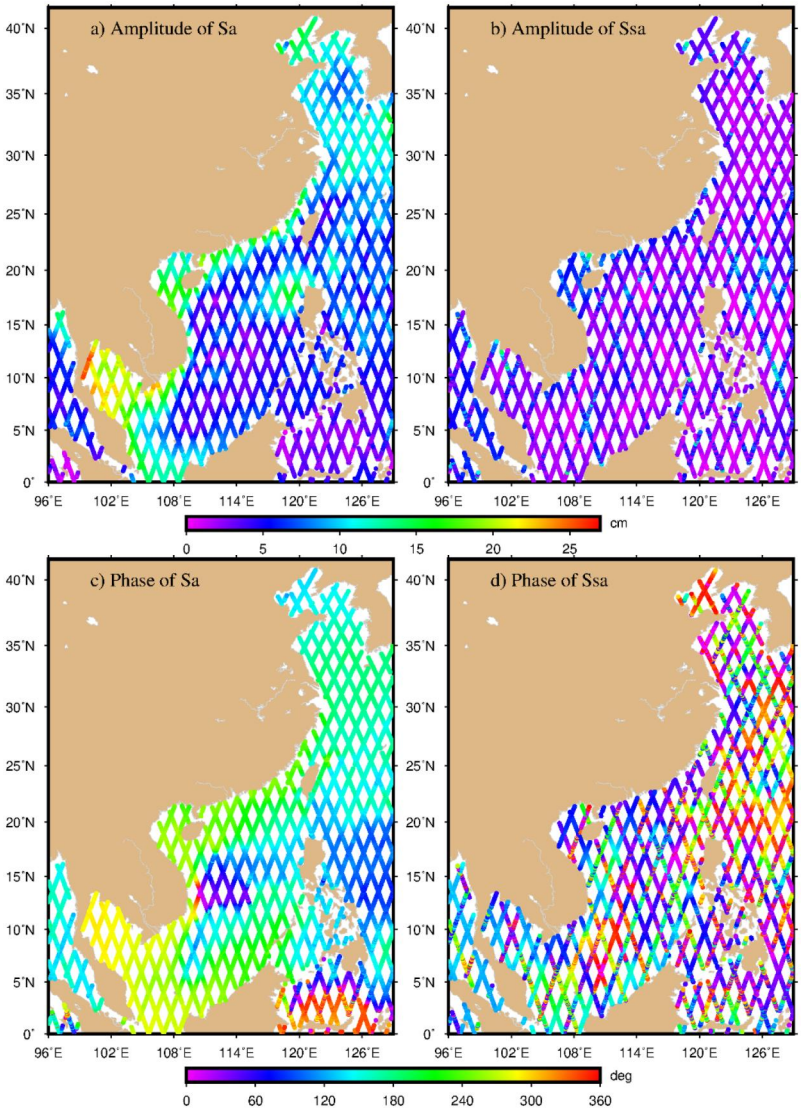

Figure 2. The along-track distribution of satellite-derived amplitude and phase of Sa and Ssa tidal constituents.

where L is the TLT value. min[·] is the function of minimize operator, H and g are the amplitude and phase of each tidal constituent, respectively, f is the focus factor of each constituent. And φ is the variable parameter of each tidal constituent. According to the equilibrium relationship between tidal components, R_1, R_2, R_3, α_1, α_2, and α_3 are the custom variables by an approximate hypothesis:

$$R_1 = \sqrt{\left((fH)_{M_2}\right)^2 + \left((fH)_{O_1}\right)^2 + 2(fH)_{M_2}(fH)_{O_1}\cos\left(\varphi_{K_1} + a_1\right)} \tag{2}$$

$$R_2 = \sqrt{\left((fH)_{S_2}\right)^2 + \left((fH)_{P_1}\right)^2 + 2(fH)_{S_2}(fH)_{P_1}\cos\left(\varphi_{K_1} + a_2\right)} \tag{3}$$

$$R_3 = \sqrt{\left((fH)_{N_2}\right)^2 + \left((fH)_{Q_1}\right)^2 + 2(fH)_{N_2}(fH)_{Q_1}\cos\left(\varphi_{K_1} + a_3\right)} \tag{4}$$

$$\begin{aligned} a_1 &= g_{K_1} + g_{O_1} - g_{M_2} \\ a_2 &= g_{K_1} + g_{P_1} - g_{S_2} \\ a_3 &= g_{K_1} + g_{Q_1} - g_{N_2} \\ a_4 &= 2g_{K_1} - 180^\circ - g_{K_2} \end{aligned} \tag{5}$$

Based on the relationship between basic astronomical elements, the φ of M_4, MS_4, M_6, Sa, and Ssa tidal constituents are calculated by the following Equations:

$$\varphi_{M_4} = 2\varepsilon_1 + 2g_{M_2} - g_{M_4} \tag{6}$$

$$\varphi_{MS_4} = \varepsilon_1 + \varepsilon_2 + g_{M_2} + g_{S_2} - g_{MS_4} \tag{7}$$

$$\varphi_{M_6} = 3\varepsilon_1 + 180^\circ + 3g_{M_2} - g_{M_6} \tag{8}$$

$$\varphi_{S_a} = \varphi_{K_1} - \frac{1}{2}\varepsilon_2 + g_{K_1} - \frac{1}{2}g_{S_2} - g_{S_a} - 180^\circ \tag{9}$$

$$\varphi_{S_a} = 2\varphi_{K_1} - \varepsilon_2 + 2g_{K_1} - g_{S_2} - g_{S_{Sa}} \tag{10}$$

Where ε_1 and ε_2 are calculated:

$$\varepsilon_1 = \tan^{-1}\frac{(fH)_{O_1}\sin\left(\varphi_{K_1} + a_1\right)}{(fH)_{M_2} + (fH)_{O_1}\cos\left(\varphi_{K_1} + a_1\right)} \tag{11}$$

$$\varepsilon_2 = \tan^{-1}\frac{(fH)_{P_1}\sin\left(\varphi_{K_1} + a_2\right)}{(fH)_{S_1} + (fH)_{P_1}\cos\left(\varphi_{K_1} + a_2\right)} \tag{12}$$

In the tidal harmonic function, f generally means the moon's nodal modulation and is the time dependent variable in 18.6-year period. In the calculation of the TLT value, the f value of each tidal constituent was determined depending on the tidal regime (the equation for F), as listed in Table 3, namely:

$$F = (H_{O_1} + H_{K_1})/M_{M_2} \tag{13}$$

Table 3. Determination of f in each tidal constituent.

Tidal constituent	$F > 4$	$0 < F \leq 0.5$
Q_1	1.183	0.807
O_1	1.183	0.806
P_1	1.000	1.000
K_1	1.113	0.882
N_2	0.963	1.038
M_2	0.963	1.038
S_2	1.000	1.000
K_2	1.317	0.748
M_4	0.928	1.077
MS_4	0.963	1.038
M_6	0.894	1.118

where H_{O1}, H_{K1}, and H_{M2} is the amplitude of O_1, K_1, and M_2, respectively. When $0.5<F\leq 4$, the TLT value should be calculated by the two types of f value, and the maximum value is taken as the finally TLT value at that location.

Calculation of ellipsoid-based TLT model

The calculation of the ellipsoid-based TLT model in this study is based on the spatial relationship between the TLT surface and the China Geodetic Coordinate System 2000 (CGCS2000) ellipsoid surface. This spatial relationship is illustrated in Figure 3. This process involves utilizing the gridded TLT values and the mean sea surface (MSS) height model to compute the distance between the TLT and the CGCS2000 surface, resulting in the formulation of the ellipsoid-based TLT model.

Figure 3 illustrates key parameters utilized in maritime cartography, where *MSL* represents the geodetic altitude at mean sea level, *TLT* signifies the distance between the TLT and MSS surface. Additionally, D_{TLT} represents the TLT datum based water depth, while $D_{CGCS2000}$ denotes the CGCS2000 surface based water depth. The conversion between D_{TLT} and $D_{CGCS2000}$ is articulated in Equation (14). Moreover, the distance between the TLT and CGCS2000 surfaces, denoted as $SEP_{TLT/CGCS2000}$, and the fundamental principle of the tide-free model are jointly governed by Equation (15).

$$D_{TLT} = D_{CGCS2000} + SEP_{TLT/CGCS2000} \tag{14}$$

$$SEP_{TLT/CGCS2000} = MSL - TLT \tag{15}$$

The *MSL* and *TLT* values are derived from the MSS and TLT model, respectively, in order to establish a conversion model for the *SEP*. Through

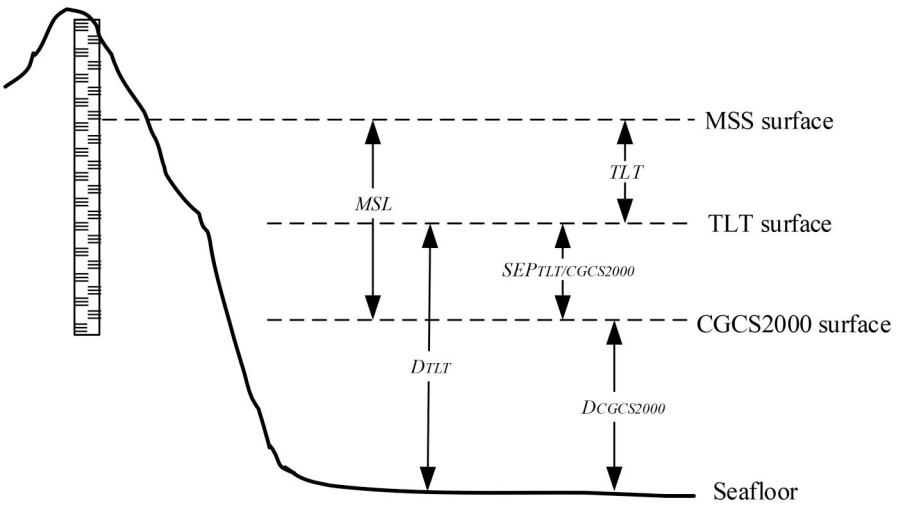

Figure 3. Spatial relationships between chart datum and reference ellipsoid surfaces.

these procedures, a precise and uninterrupted model for TLT-to-CGCS2000 is formulated for the study area.

It is noteworthy that different MSS models are based on different reference ellipsoids. Since this study adopts the CGCS2000 reference ellipsoid, MSS heights derived from models based on other reference ellipsoids (e.g. WGS84) must be converted to the CGCS2000 framework prior to their application. This conversion is a critical step to ensure the usability and consistency of the ellipsoid-based TLT model.

Empirical tide model of long-period tidal constituents

The empirical tidal model for the Sa and Ssa constituents was developed based on satellite-derived data. However, due to the phase values ranging from 0° to 360°, conventional interpolation methods cannot be directly applied during the gridding process. To address this issue, two parameters, the sine variable *HS* and cosine variable *HC* of the amplitude, were introduced to linearize the amplitude and phase, expressed as:

$$HS = H \cdot sinG \tag{16}$$

$$HC = H \cdot cosG \tag{17}$$

where H and G are the amplitude and phase of each tidal constituent, respectively. Utilizing the inverse distance to a power interpolation method, a parameter model with a spatial resolution of $1/8^\circ \times 1/8^\circ$ was developed. Notably, the amplitude and phase values at grid points were computed to construct an empirical model. Figure 4 illustrates the spatial distribution of tidal amplitudes and phases for Sa and Ssa.

The spatial amplitude distribution exhibits a smooth pattern. In Figure 4a, the tide gauge results surpass the model results notably in the central Bohai Sea and the Yellow Sea (further referred to as BY Sea), a semi-enclosed region in China. Research has previously highlighted that the satellite altimetry data in this area are greatly influenced by interaction of radar signal and land topography, leading to reduce measurement efficiency (Peng et al. 2023). Furthermore, there is a stronger dependency on long-period tidal constituents in relation to the timescale data, contributing to lower precision in the inversion process. It is worth noting that the amplitude of Sa and Ssa tides is higher in coastal regions compared to open waters, with notable variations across different sea areas.

Analyzing the distribution and statistical data of long-period tidal constituents in Figure 4a, the amplitude of Sa varies between 1.01 and 19.88 cm. Approximately 57.68% of the data points fall within the 5–10 cm range, while 25.06% exceed 10 cm. The highest amplitude value is recorded in the northern part of the South China Sea at 23.66°N, 117.56°E. Larger

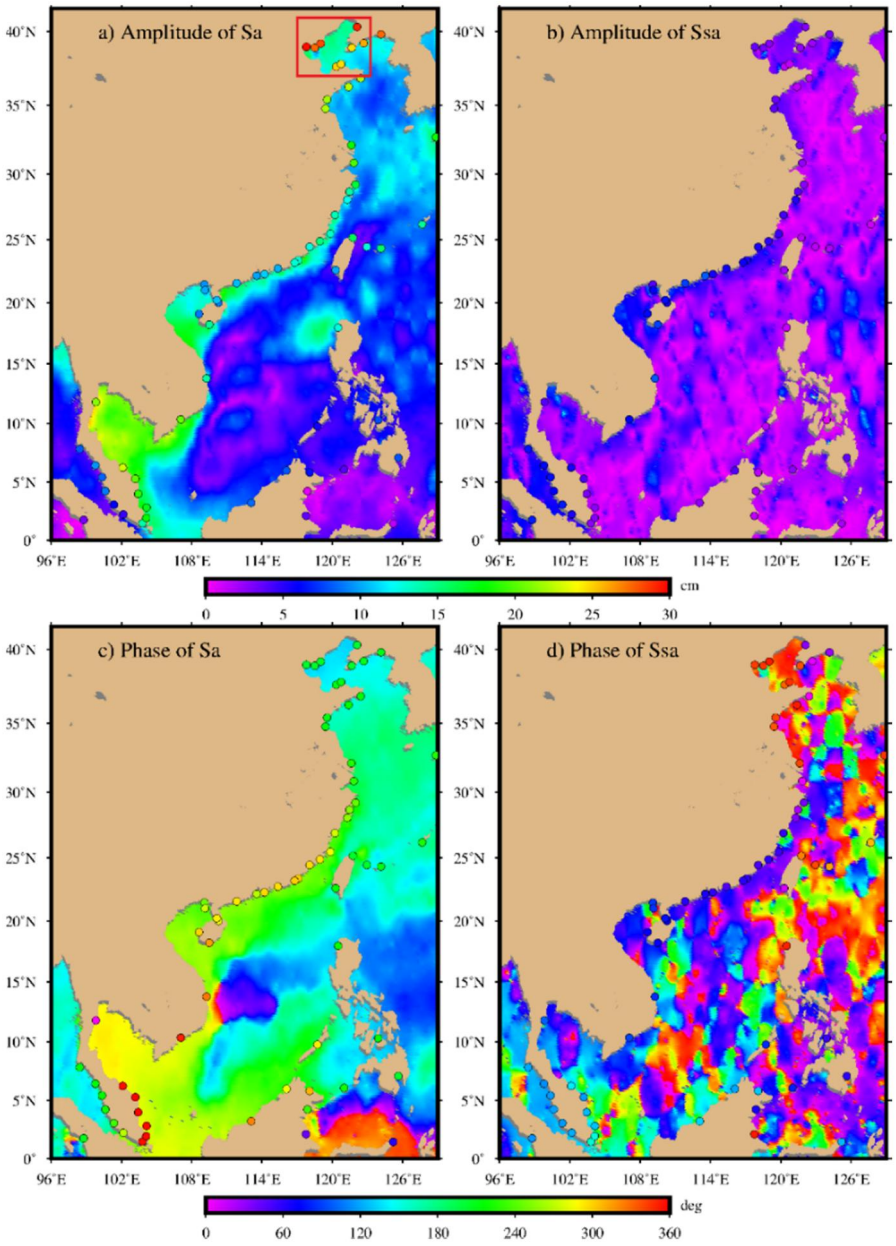

Figure 4. The empirical model of Sa and Ssa in the study area. The tide gauge stations records are shown as colored dots.

values are predominantly found in the Gulf of Tonkin and the BY Sea. In contrast, the amplitude of Ssa (Figure 4b) ranges from 0.04 to 9.91 cm, with 94% of the points below 5 cm. An intriguing observation is the significantly larger amplitude of the Sa tide in the northeastern open waters of the South China Sea, particularly adjacent to the Philippines, compared to

surrounding regions. This spatial disparity may be linked to ENSO variability, though the exact mechanisms require further investigation.

The phase distribution of the long-period tidal constituents extracted from satellite altimetry exhibits a relatively uniform pattern, with a singular amphidromic point of the Sa constituent located in the central South China Sea. This singular amphidromic point represents a location in the tidal system where the tidal amplitude approaches zero and the phase experiences a rapid transition. Such points are uncommon for Sa and Ssa constituents due to their long wavelengths, highlighting the unique tidal dynamics in this region. In contrast, the phase distribution of Ssa exhibits greater complexity, likely due to its smaller amplitude.

Figure 5 presents the amplitude results for Sa and Ssa tidal constituents at 72 tide gauge stations, comparing with the empirical model from this study, the EOT20, and the FES2014 models. It is evident that, for both the Sa and Ssa constituents, the results from this study's empirical model align better with the tide gauge observations, with generally smaller difference than those of the EOT20 and FES2014 models. Moreover, the Sa results from the EOT20 model are closer to the tide gauge data compared to the FES2014 model. It is important to point out that the FES2014 model's Sa tidal amplitude results are essentially zero, and for the Ssa constituent, the maximum amplitude in both the EOT20 and FES2014 models reaches only 0.77 cm, showing a significant discrepancy with the corresponding tide gauge results. Therefore, when utilizing the Sa and Ssa results from these models, it is necessary to consider their accuracy (Xu et al. 2024).

Table 4 presents the statistical differences of the amplitude of the Sa and Ssa constituents between the tide gauge results and those from this study's empirical model, EOT20, and FES2014 model. Given that the FES2014

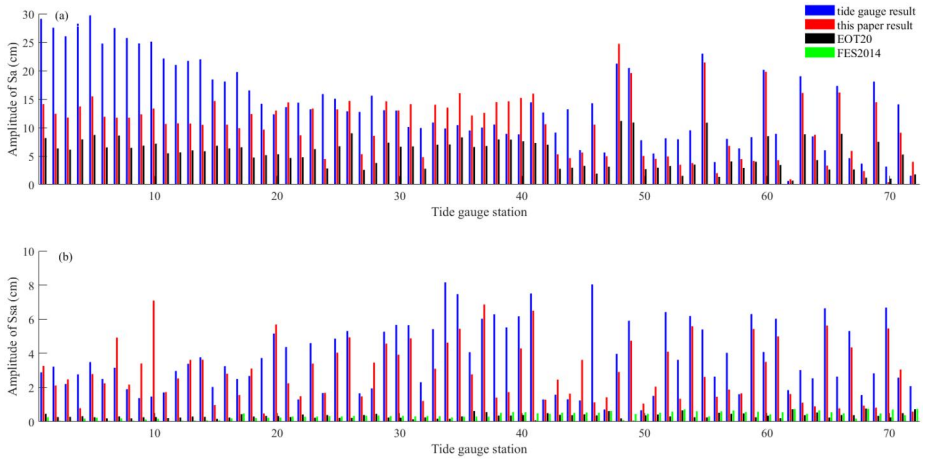

Figure 5. The amplitude of Sa and Ssa for tide gauge result, the empirical model result, EOT20 and FES2014.

Table 4. Statistical differences between tide gauge result and those from this paper result and tide model results (cm).

	Sa constituent				Ssa constituent			
Model type	average	SD	max	min	average	SD	max	min
This paper result	3.72	5.85	15.75	−6.41	0.77	1.67	6.91	−5.61
EOT20	8.64	5.97	21.21	−0.23	3.40	2.04	7.99	0.09
FES2014	14.16	7.27	29.68	0.62	3.37	1.97	7.91	0.08

model demonstrates higher RSS values than FES2022 in the study area, we chose to focus on FES2014 for comparison purposes. These differences quantify the level of agreement or discrepancy between the tide gauge observations and the model predictions, providing a clearer understanding of how well each model performs relative to real-world measurements. For Sa constituents, the average and standard deviation (SD) values of the difference between tide gauge-derived and empirical model results are 3.72 and 5.85 cm, respectively. In comparison, they reach 8.64 and 5.97 cm for tide gauge-derived and EOT20 results, which show better performance than FES2014. For the Ssa constituent, the average difference and standard deviation between the tide gauge-derived values and the empirical model were 0.77 and 1.67 cm, respectively, indicating higher precision compared to both the EOT20 and FES2014 models. Notably, the Ssa amplitude in the EOT20 model is less than 1 cm, which highlights the limitations of directly relying on EOT20 for Ssa results. This underscores the importance of incorporating satellite-derived data in the development of empirical models.

Selection of tide model

The study assesses the accuracy of four tide models, namely FES2014, FES2022, EOT20, and DTU16, by comparing them with 72 tide gauge observations. Discrepancies in spatial resolution among the models result in the presence of unreliable grid points in close proximity. Previous research has demonstrated that the method of interpolation significantly impacts result accuracy. To address this issue, a meticulous algorithm is introduced in this study. It identifies grid points corresponding to tide gauge locations within the models and employs the spline spatial interpolation method to guarantee data continuity and accuracy. This approach effectively mitigates spatial discontinuity arising from differing spatial resolutions of the models. Not only does this method enhance the precision of harmonic constants extraction, but it also boosts the credibility of assessment outcomes.

Table 5 presents the root-mean-square (RMS) error values for each model pertaining to the eight tidal constituents, along with the total root

Table 5. RMS and RSS between tide models and tide gauge results (cm). The second row of each model is the result after excluding the second tide gauge station.

Tide model	Q_1	O_1	P_1	K_1	N_2	M_2	S_2	K_2	M_4	RSS
FES2014	0.59	2.36	0.96	2.61	1.47	6.62	3.04	1.25	1.94	8.40
	0.58	2.28	0.94	2.50	1.32	5.35	2.81	1.20	1.93	7.24
FES2022	0.51	2.30	0.96	2.31	1.88	8.94	3.55	1.56	3.13	10.50
	0.50	2.09	0.93	2.15	1.17	5.41	2.21	1.10	2.23	6.84
EOT20	0.44	1.75	0.79	1.92	1.30	6.28	3.06	0.97	2.05	7.68
	0.43	1.69	0.77	1.88	1.14	5.16	2.77	0.91	2.04	6.61
DTU16	0.52	1.77	1.44	2.28	1.59	6.25	2.90	1.23	–	7.89
	0.51	1.77	1.35	2.25	1.53	5.66	2.70	1.12		7.30

sum square (RSS) error for these constituents. The assessment of individual tidal components' accuracy reveals that the EOT20 model exhibited superior precision across most constituents. The EOT20 model demonstrates an RSS value of 7.68 cm, signifying its superior overall accuracy. Subsequently, the DTU16 exhibits an RSS value of 7.89 cm, while the FES2014 shows a value of 8.40 cm. The precision of the various tide models exhibited notable disparities. Despite exhibiting satisfactory performance at certain points, the FES2014 model's overall margin of error remained substantial. Conversely, the RSS value for the FES2022 model stood at 10.50 cm, a noteworthy deviation from tide gauge measurements when compared to the FES2014 model. The EOT20 and DTU16 models demonstrated comparable performance levels. This comparative evaluation not only enhances our comprehension of the models' performance in distinct areas but also furnishes a scientific groundwork that provides a scientific basis for the improvement and optimization of future models.

For the shallow water tidal constituents, it was observed that while FES2022 represents the latest model in the FES series, its stability in certain regions was not as robust as that of FES2014. Specifically, for the M_4 constituent, the RMS values between FES2014 and tide gauge results were 1.94 cm, whereas those for FES2022 were 3.13 cm, indicating reduced stability in certain regions. Furthermore, the RMS values derived from EOT20 and FES2014 were nearly identical, measuring 2.05 and 1.94 cm, respectively. Although EOT20 exhibited superior performance for primary tidal constituents, its results for shallow water constituents in the study area did not demonstrate a clear advantage over FES2014. Consequently, FES2014 was selected for providing shallow water constituents results in this study due to its greater stability and consistent performance in the region, as well as its nearly equivalent accuracy to EOT20 for the M_4 constituent, making it a reliable choice for the analysis.

During our data processing, we identified a significant discrepancy at the second tide gauge station (39.82°N, 124.15°E), as shown in Figure 1, between the FES2022 model and both the tide gauge measurements and the outputs from other tide models. To minimize the potential influence of

Table 6. The amplitide of M_2 and K_2 at the second tide gauge station extracted from tide models and tide gauge result (cm).

Tidal constituents	FES2014	FES2022	EOT20	DTU16	Tide gauge
M_2	211.40	156.80	206.18	214.16	219.79
K_2	20.80	9.70	20.24	21.88	20.81

spatial interpolation methods, we directly extracted the model values from the nearest grid point to the tide gauge station. The amplitude values of the M_2 and S_2 tidal constituents for the tide models and the tide gauge result are presented in Table 6, where a notable deviation in the FES2022 model compared to other models is evident at this location.

To evaluate the overall impact of this discrepancy, we recalculated the RMS and RSS values for the tide models after excluding this tide gauge station, with the updated results displayed in the second row of each model in Table 5. Results indicate that, after removing this station, the RSS value for the EOT20 model improved from 7.68 to 6.61 cm, maintaining its position as the most accurate model. Similarly, the RSS value for the FES2022 model improved significantly, decreasing from 10.50 to 6.84 cm, surpassing the accuracy of the FES2014 and DTU10 models.

These findings suggest that the regional discrepancy at this specific station significantly impacts the overall accuracy of the FES2022 model in the study area. The considerable deviations emphasize the importance of thoroughly evaluating model performance, particularly in regions where such anomalies occur. This observation highlights the need for further refinement and localized adjustments to the FES2022 model to enhance its reliability and accuracy across different regions.

Determination of ellipsoid-based TLT datum model

A hybrid tide model incorporating 13 tidal constituents was established based on validation results against tide gauge stations in the China Seas. These constituents include short-period components from EOT20 (8) and FES2014 (3), as well as two long-period constituents derived from satellite data. The MSS-based TLT model was constructed by calculating the TLT values at each grid point of the hybrid tide model using Equation (1). Figure 6 presents the spatial distribution of TLT values in the study area, where the color gradient represents the spatial variation of TLT values, and the contours provide a detailed depiction of their distribution.

The distribution reveals that the TLT values ranges from 25.54 to 460.78 cm in the China Seas, contrasting with the lower value, typically below 150 cm, observaed in the central South China Sea, the eastern Philippines, and the Java Sea. This distinct pattern underscores the diverse impact of tidal forces across the study areas.

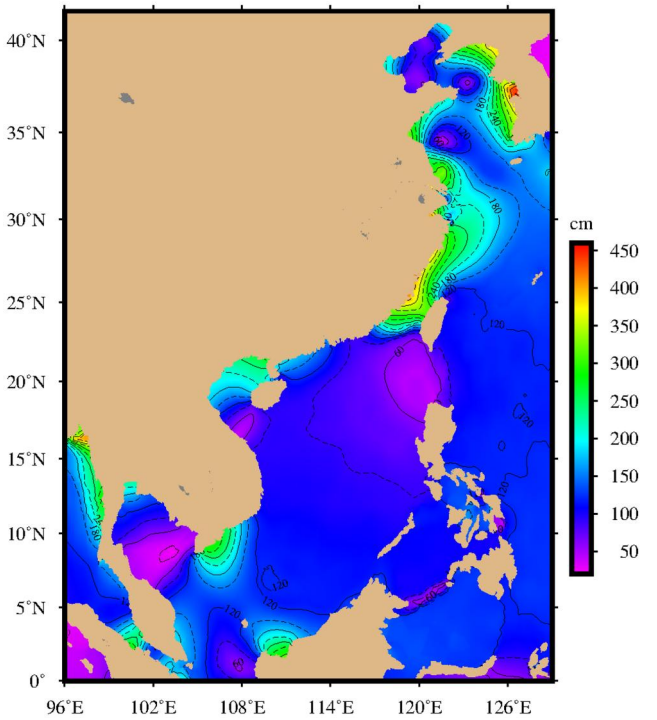

Figure 6. Distribution of TLT values with respect to mean sea surface.

Specifically, the higher TLT values along the East China Sea coast may be due to the larger tidal amplitude in that region. In contrast, the lower TLT values in the central South China Sea and eastern Philippine regions indicate that tidal variations in these regions are more subdued (Fang et al. 2004). However, there may be uncertainty within this distribution. For example, in shallow nearshore areas, the variation of the TLT may be affected by river inflow, sediment transport, and human activities, resulting in prediction errors in tidal amplitude. In addition, the spatial resolution of the model and the accuracy of the input data may also affect the calculation results of the TLT values, especially in areas with complex topography, where certain deviations may exist. Therefore, when applying these TLT model result, it is necessary to validate and calibrate them with the field measurements to ensure the accuracy.

The latest hybrid MSS model, developed in 2023 (HYBRID2023MSS), was chosen to develop the CCGS2000 elliposid based TLT model, which is motivated by its high resolution, incorporation of up-to-date satellite data, enhanced accuracy in coastal and shelf areas, and advanced data assimilation technique, offering notable advantages over DTU18 and Centre National d'Études Spatiales (CNES20) MSS model. We first extract the MSS results of the HYBRID2023MSS at the grid points of the EOT20 model to ensure that the two models have the same spatial resolution. It is

worth noting that the HYBRID2023MSS model is based on WGS84 as the reference datum, which needs to be converted to CGCS2000 surface. Finally, using Equation (14), the ellipsoid-based TLT model can be obtained. Figure 7 presents the distribution of deviation between the TLT surface and the CGCS2000 surface in China Seas.

The deviation between TLT surface and CGCS2000 ranges from −53.44 to 74.50 m, exhibiting significant spatial variations, particularly in the East China Sea and South China Sea regions.

The BY Sea regions display relatively low and uniform deviations, attributable to the shallow and flat terrain in these areas. The continental shelf of the East China Sea shows lower deviations, which increase with distance, forming a clear gradient. This pattern is mainly due to the significant tidal influence in the shallow continental shelf areas, resulting in lower sea surface heights and thus smaller deviations from the CGCS2000 surface. In contrast, in the deep-water areas of the East China Sea, the sea surface height increases, leading to significantly higher deviations.

The deviation distribution in the South China Sea is more complex. The northern continental shelf shows lower deviations, whereas the southern deep-water basin exhibits significantly higher deviations. The lower deviations in the northern continental shelf are due to the enhanced tidal dynamics in shallow waters with complex topography, resulting in lower

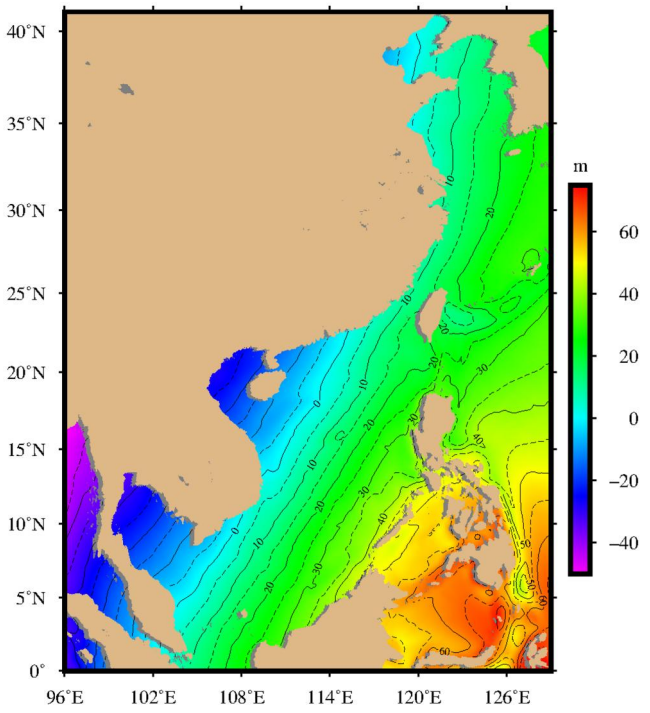

Figure 7. The distribution of deviation between TLT surface and CGCS2000 reference surface.

sea surface heights. Conversely, the deep-water areas of the South China Sea, characterized by greater depths and reduced tidal dynamics, have higher sea surface heights, resulting in increased deviations (Li et al. 2024). Climate change impacts sea level rise, further affecting sea surface height, and deviation distribution. Global warming-induced sea level rise and thermal expansion have a significant impact on the deviations, particularly in the coastal areas of the East China Sea and South China Sea (Zhou et al. 2022). The varying influence of these factors in different regions results in the significant spatial differences in deviations.

Discussion

The accuracy of the MSS based TLT model was evaluated using TLT values calculated at 72 tide gauge stations. Figure 8 shows the statistical TLT values and the discrepancies between the tide gauge observations and the MSS based TLT model results. The MSS based TLT model results demonstrate a consistent spatial distribution and magnitude when compared to tide gauge measurements. The differences range from −12.24 to 55.70 cm, with a SD of 14.68 cm. Notably, the SD values calculated using EOT20 and FES2014 are 15.30 and 15.86 cm, respectively. Additionally, approximately 51% of the stations show differences within ±15 cm, and 31% fall within ±10 cm. Furthermore, 92% of the stations show positive differences, indicating that the TLT values derived from tide gauge observations are generally higher than those from TLT model. As discussed above, the tidal constituent amplitudes in the hybrid model are generally smaller than those observed at tide gauge stations. Consequently, this leads to higher TLT values in the

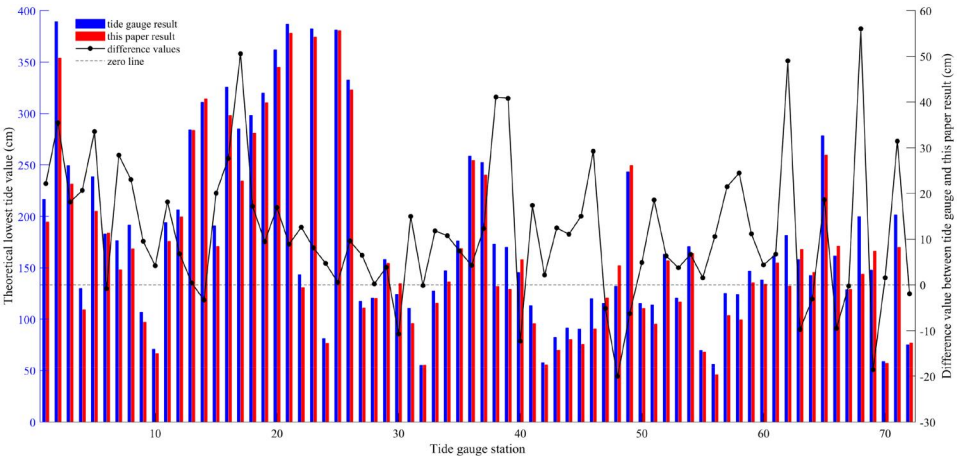

Figure 8. Statistical results and the difference values between MSS based TLT model and tide gauge result. Left *y*-axes is the TLT value and the right y-axes the difference between tide gauge stations and TLT model.

tide gauge observations compared to TLT model. Although the MSS based TLT model demonstrates good accuracy in the study area, its performance should be reassessed using local data in future applications to ensure precision.

This study presents a comprehensive solution for establishing a continuous TLT surface in the study area and enhancing the accuracy of the TLT model through the integration of multiple tide models and satellite data. Despite these advancements, several limitations warrant attention. First, the accuracy of satellite altimetry data in nearshore areas remains an unavoidable challenge. Conventional and SAR nadir altimetry are constrained by the wide separation between satellite ground tracks and the 7 km radius of the radar beam in the cross-track direction. This spatial resolution is insufficient for accurately capturing tidal dynamics in shallow coastal (Brown et al. 2023). As a result, tides in the coastal regions are significantly larger and more spatially variable than in the open ocean (Hart-Davis et al. 2024). However, the continuous accumulation of SWOT satellite data provides a promising data foundation for improving accuracy in nearshore regions. Secondly, the acquisition of harmonic constants is closely related to the duration of tidal observations, often exhibiting a trend of variation (Bij de Vaate, Slobbe, and Verlaan 2022). Consequently, the CD model established based on these constants cannot effectively accommodate long-term changes. Thirdly, the CD model constructed using tidal models are static and precise; however, with ongoing sea level rise and the increasing frequency of extreme weather events, the need for developing a dynamic depth datum is becoming more urgent. Overcoming these limitations is crucial for refining the accuracy and applicability of the CD model.

Conclusions

This paper introduces a novel approach to develop a CD model using global tide models and satellite-derived long-period tidal constituents. Short-period tidal constituents in global ocean tide models exhibit regional variations in accuracy, with limited models offering long-period tidal results. Four recent global tide models - FES2014, FES2022, EOT20 and DTU16 – are assessed for their accuracy in the China Seas. Results indicate that EOT20 demonstrated slightly superior precision. An empirical model for long-period tidal constituents is established using satellite-derived along-track results provided by CTOH. Comparative analysis among the empirical model presented in this study, EOT20 and FES2014 model, and tide gauge results reveals that the empirical model presented in this study more accurately represents long-period tidal constituents. Building upon this, the TLT values at each grid is calculated by integrating short-

period tidal constituents from the EOT20 model, shallow water tidal constituents from FES2014, and the developed long-period empirical model. The standard deviation of MSS based TLT model from the hybrid tide model is 14.68 cm, when compared with 72 tide gauge results, indicating higher accuracy compared to individual models.

The CGCS2000 ellipsoid based TLT model was established by utilizing the HYBRID2023MSS model. The results highlighted notable spatial discrepancies in deviation values. Furthermore, future studies should concentrate on improving the precision of observational data through augmenting the quantity of measurement locations, utilizing advanced observational tools, and refining data analysis techniques. The amalgamation of various data sources such as satellite altimetry, tide gauge observations, and numerical simulations is anticipated to enhance the accuracy of the model significantly. These endeavors are poised to play a pivotal role in advancing the creation of a more precise and dependable depth reference model, thereby establishing a more robust groundwork for marine research and practical implementations.

Acknowledgments

Satellite altimetry data used in this study were developed, validated, and distributed by the CTOH/LEGOS, France. The authors would like to acknowledge the CTOH for providing the satellite-derived harmonic constants of tidal constituents, TICON data set provide the harmonic constants.

Author contributions

Conceptualization: Y. L., and M. K. Methodology: Y. F. Validation: Y. F., Q. T., and X. D. Formal analysis: Y. F. Investigation: F. P., L. Y., and L. C. Writing – original draft preparation: Y. F., Y. L. and X. D. Writing – review and editing: M. K., Q. T., and X. M. All authors have read and agreed to the published version of the manuscript.

Disclosure statement

No potential conflict of interest was reported by the authors.

Funding

This research was funded by the Basic Scientific Fund for National Public Research Institutes of China (No. 2023Q05); the National Natural Science Foundation of China (No. 42376185, 42404052, and 42104035); the Shandong Provincial Natural Science Foundation of China (ZR2023MD073). The first author is grateful for the financial support provided by the Program of China Scholarship Council (No. CSC 202104180021).

References

Avşar, N. B., and Ş. Kutoğlu. 2020. "Recent Sea Level Change in the Black Sea from Satellite Altimetry and Tide Gauge Observations." *ISPRS International Journal of Geo-Information* 9 (3): 185. https://doi.org/10.3390/ijgi9030185

Azkue, M., E. Onofrio, and L. Banegas. 2021. "Development of an Empirical Chart Datum Model for A Region of the Southwest Atlantic Ocean." *Ocean and Coastal Research* 69: 1–11. https://doi.org/10.1590/2675-2824069.21-028mfda

Bij de Vaate, I., D. C. Slobbe, and M. Verlaan. 2022. "Secular Trends in Global Tides Derived from Satellite Radar Altimetry." *Journal of Geophysical Research: Oceans* 127 (10): e2022JC018845. https://doi.org/10.1029/2022JC018845

Birol, F., N. Fuller, F. Lyard, M. Cancet, F. Niño, C. Delebecque, S. Fleury, F. Toublanc, A. Melet, M. Saraceno, and F. Léger. 2017. "Coastal Applications from Nadir Altimetry: Example of the X-TRACK Regional Products." *Advances in Space Research* 59 (4): 936–953. https://doi.org/10.1016/j.asr.2016.11.005

Cheng, Y., and O. B. Andersen. 2011. "Multimission Empirical Ocean Tide Modeling for Shallow Waters and Polar Seas." *Journal of Geophysical Research: Oceans* 116 (C11): C11001. https://doi.org/10.1029/2011JC007172

Desportes, C., E. Obligis, and L. Eymard. 2007. "On the Wet Tropospheric Correction for Altimetry Coastal Regions." *IEEE Transactions on Geoscience and Remote Sensing* 45 (7): 2139–2149. https://doi.org/10.1109/TGRS.2006.888967

Deng, X., and W. E. Featherstone. 2006. "A Coastal Retracking System for Satellite Radar Altimeter Waveforms: Application to ERS-2 around Australia." *Journal of Geophysical Research: Oceans* 111 (C6): C06012. https://doi.org/10.1029/2005JC003039

Egbert, G. D., and S. Y. Erofeeva. 2002. "Efficient Inverse Modeling of Barotropic Ocean Tides." *Journal of Atmospheric and Oceanic Technology* 19 (2): 183–204. 0426(2002)019 https://doi.org/10.1175/1520-594

Erofeeva, S., L. Padman, and L. Howard. 2020. "Tide Model Driver (TMD) version 2.5, Toolbox for MATLAB." Retrieved from https://www.github.com/EarthAndSpaceResearch/TMD_Matlab_Toolbox_v2.5

Fang, G., Y. K. Kwok, K. Yu, and Y. Zhu. 2004. "Numerical Simulation of Principal Tidal Constituents in the South China Sea, Gulf of Tonkin, and Gulf of Thailand." *Continental Shelf Research* 24 (17): 2019–2044. https://doi.org/10.1016/j.csr.2004.06.007

Feng, Y., Y. Fu, L. Yang, and D. Zhou. 2023. "Contributions of Annual and Semiannual Tidal Constituents to Chart Datum in the China Seas and Adjacent Waters." *Acta Oceanologica Sinica* 42 (10): 127–136. https://doi.org/10.1007/s13131-023-2231-5

Fok, H. S. 2012. *Ocean Tides Modeling using Satellite Altimetry*. Columbus, OH, USA: The Ohio State University.

Haigh, I. D., M. Marcos, S. A. Talke, P. L. Woodworth, J. R. Hunter, B. S. Hague, A. Arns, E. Bradshaw, and P. Thompson. 2023. "GESLA Version 3: A Major Update to the Global Higher-Frequency Sea-Level Dataset." *Geoscience Data Journal* 10 (3): 293–314. https://doi.org/10.1002/gdj3.174

Hart-Davis, M. G., G. Piccioni, D. Dettmering, C. Schwatke, M. Passaro, and F. Seitz. 2021. "EOT20: A Global Ocean Tide Model from Multi-Mission Satellite Altimetry." *Earth System Science Data* 13 (8): 3869–3884. https://doi.org/10.5194/essd-13-3869-2021

Hart-Davis, M. G., O. B. Andersen, R. D. Ray, E. D. Zaron, C. Schwatke, R. L. Arildsen, D. Dettmering, and K. Nielsen. 2024. "Tides in Complex Coastal Regions: Early Case Studies from Wide-Swath SWOT Measurements." *Geophysical Research Letters* 51 (20): e2024GL109983. https://doi.org/10.1029/2024GL109983

Iz, H. B., and C. K. Shum. 2022. "Minimum Record Length for Detecting A Prospective Uniform Sea Level Acceleration at A Tide Gauge Station." *All Earth* 34 (1): 8–15. https://doi.org/10.1080/27669645.2022.2045697

Li, Y., L. Mu, D. You, J. Wang, Q. Niu, and X. Liao. 2024. "Changes in Sea Level Along the South China Sea Coast Based on the Homogenized Tide Gauge Data." *Journal of Marine Science and Engineering* 12 (3): 478. https://doi.org/10.3390/jmse12030478

Lyard, F. H., D. J. Allain, M. Cancet, L. Carrère, and N. Picot. 2021. "FES2014 Global Ocean Tide Atlas: Design and Performance." *Ocean Science* 17 (3): 615–649. https://doi.org/10.5194/os-2020-96

Lyard, F., F. Lefevre, T. Letellier, and O. Francis. 2006. "Modelling the Global Ocean Tides: Modern Insights from FES2004." *Ocean Dynamics* 56 (5-6): 394–415. https://doi.org/10.1007/s10236-006-0086-x

Madsen, K. S., J. L. Høyer, and C. C. Tscherning. 2007. "Near-Coastal Satellite Altimetry: Sea Surface Height Variability in the North Sea-Baltic Sea Area." *Geophysical Research Letters* 34 (14): L14601. https://doi.org/10.1029/2007GL029965

National Standards of China. 2023. *Specifications for Hydrographic Surveying (GB12327–2022)*. Beijing: Standards Press of China.

Pan, H., J. Sun, T. Xu, and Z. Wei. 2024. "Extraction of Ocean Tides in the Bohai Sea from GFO Satellite Altimeter via A Modified Tidal Harmonic Analysis Algorithm." *Continental Shelf Research* 276: 105231. https://doi.org/10.1016/j.csr.2024.105231

Peng, F., X. Deng, M. Jiang, S. Dinardo, and Y. Shen. 2023. "A New Method to Combine Coastal Sea Surface Height Estimates from Multiple Retrackers by Using the Dijkstra Algorithm." *Remote Sensing* 15 (9): 2329. https://doi.org/10.3390/rs15092329

Piccioni, G., D. Dettmering, W. Bosch, and F. Seitz. 2019. "TICON: TIdal CONstants Based on GESLA Sea-Level Records from Globally Located Tide Gauges." *Geoscience Data Journal* 6 (2): 97–104. https://doi.org/10.1002/gdj3.72

Ray, R. D. 1999. "A Global Ocean Tide Model from TOPEX/POSEIDON Altimetry, GOT99.2." *NASA/TM—1999-209478*. Greenbelt, MD: Goddard Space Flight Center, 58.

Savcenko, R., W. Bosch, D. Dettmering, and F. Seitz. 2012. "EOT11a – Global Empirical Ocean Tide Model from Multi-Mission Satellite Altimetry." *PANGAEA* : 8949. https://doi.org/10.1594/PANGAEA.834232.

Stammer, D., R. D. Ray, O. B. Andersen, B. K. Arbic, W. Bosch, L. Carrère, Y. Cheng, D. S. Chinn, B. D. Dushaw, G. D. Egbert, et al. 2014. "Accuracy Assessment of Global Barotropic Ocean Tide Models." *Reviews of Geophysics* 52 (3): 243–282. https://doi.org/10.1002/2014RG000450

Sun, W., X. Zhou, D. Zhou, and Y. Sun. 2022. "Advances and Accuracy Assessment of Ocean Tide Models in the Antarctic Ocean." *Frontiers in Earth Science* 10: 757821. https://doi.org/10.3389/feart.2022.757821

Turner, J., J. C. Iliffe, M. Ziebart, A. J. Talbot, and A. P. Lessnoff. 2013. "Accuracy of Vertical Datum Surfaces in Coastal and Offshore Zones." *Survey Review* 45 (331): 254–262. https://doi.org/10.1179/1752270613Y.0000000040

Turner, J., J. C. Iliffe, M. Ziebart, C. Wilson, and K. Horsburgh. 2010. "Interpolation of Tidal Levels in the Coastal Zone for the Creation of a Hydrographic Datum." *Journal of Atmospheric and Oceanic Technology* 27 (3): 605–613. https://doi.org/10.1175/2009JTECHO645.1

Varbla, S., J. Ågren, A. Ellmann, and M. Poutanen. 2022. "Treatment of Tide Gauge Time Series and Marine GNSS Measurements for Vertical Land Motion with Relevance to the Implementation of the Baltic Sea Chart Datum 2000." *Remote Sensing* 14 (4): 920. https://doi.org/10.3390/rs14040920

Woodworth, P. L., J. R. Hunter, M. Marcos, P. Caldwell, M. Menéndez, and I. Haigh. 2016. "Towards A Global Higher-Frequency Sea Level Dataset." *Geoscience Data Journal* 3 (2): 50–59. https://doi.org/10.1002/gdj3.42

Xu, X., H. Pan, F. Teng, G. Fang, and Z. Wei. 2024. "A Comparison of Global and Regional Ocean Tide Models with Tide Gauges in the East Asian Marginal Seas." *Journal of Sea Research* 201: 102527. https://doi.org/10.1016/j.seares.2024.102527

Zhou, D., Y. Liu, Y. Feng, H. Zhang, Y. Fu, Y. Liu, and Q. Tang. 2022. "Absolute Sea Level Changes along the Coast of China from Tide Gauges, GNSS, and Satellite Altimetry." *Journal of Geophysical Research: Oceans* 127 (9): e2022JC018994. https://doi.org/10.1029/2022JC018994